RelitLRM: Generative Relightable Radiance for Large Reconstruction Models

Tianyuan Zhang[1] **Zhengfei Kuang**[2] **Haian Jin**[3] **Zexiang Xu**[4] **Sai Bi**[4] **Hao Tan**[4]
He Zhang[4] **Yiwei Hu**[4] **Milos Hasan**[4] **William T. Freeman**[1] **Kai Zhang**[4]* **Fujun Luan**[4]*
[1]Massachusetts Institute of Technology   [2]Stanford University
[3]Cornell University   [4]Adobe Research

ABSTRACT

We propose *RelitLRM*, a Large Reconstruction Model (LRM) for generating high-quality Gaussian splatting representations of 3D objects under novel illuminations from sparse (4-8) posed images captured under unknown static lighting. Unlike prior inverse rendering methods requiring dense captures and slow optimization, often causing artifacts like incorrect highlights or shadow baking, RelitLRM adopts a feed-forward transformer-based model with a novel combination of a geometry reconstructor and a relightable appearance generator based on diffusion. The model is trained end-to-end on synthetic multi-view renderings of objects under varying known illuminations. This architecture design enables to effectively decompose geometry and appearance, resolve the ambiguity between material and lighting, and capture the multi-modal distribution of shadows and specularity in the relit appearance. We show our sparse-view feed-forward RelitLRM offers competitive relighting results to state-of-the-art dense-view optimization-based baselines while being significantly faster. Our project page is available at: https://relit-lrm.github.io/.

1 INTRODUCTION

Reconstructing high-quality, relightable 3D objects from sparse images is a longstanding challenge in computer vision, with vital applications in gaming, digital content creation, and AR/VR. This problem is typically resolved by inverse rendering systems. However, most existing inverse rendering approaches suffer from limitations ranging from requiring dense captures under controlled lighting, slow per-scene optimization, using analytical BRDF hence not capable of modeling complex light transport, lacking data prior hence failure to resolve the ambiguity between shading and lighting in the case of static unknown lighting (Ramamoorthi & Hanrahan, 2001; Zhang et al., 2021b;a; 2022a; Jin et al., 2023; Kuang et al., 2024).

To overcome these limitations, we present *RelitLRM*, a generative Large Reconstruction Model (LRM) (Zhang et al., 2024a) that efficiently reconstructs high-quality, relightable 3D objects from as few as 4–8 posed images captured under unknown lighting conditions. RelitLRM employs a feed-forward transformer-based architecture integrated with a denoising diffusion probabilistic model trained on a large-scale relighting dataset. This architecture models a multi-modal distribution of possible illumination decompositions, enabling deterministic reconstruction of object geometry and probabilistic relighting. In the case of glossy objects and challenging high-frequency novel lighting, the relit object appearance is inherently multi-modal with possibly many small specular regions; our relit appearance generator can well capture such high-frequency appearance, while regression-based approaches tend to be dominated by large smooth non-specular or weakly specular areas, and hence ignore the small strong specular highlights (see Fig. 5).

As shown in Fig. 1, our method can accurately reconstruct and relight the object's appearance under diverse lighting conditions and viewpoints, demonstrating its capability for photorealistic rendering even with limited input views. By processing tokenized input images and target lighting conditions through transformer blocks, RelitLRM decodes 3D Gaussian (Kerbl et al., 2023) primitive parameters within approximately one second on a single A100 GPU. This approach disentangles geometry,
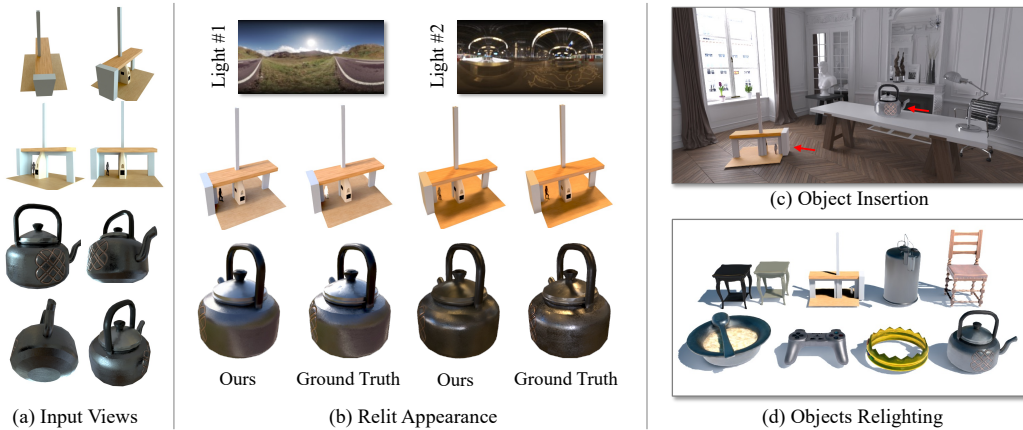
---
*Co-advise on the project

1

Figure 1: **Demonstration of *RelitLRM*'s relighting capabilities. (a)** Sparse posed images captured under unknown lighting conditions serve as the input for our method. **(b)** *RelitLRM* accurately reconstructs and relight the 3D object in the form of 3DGS under novel target lightings (either outdoor or indoor), with renderings closely matching the ground truth. **(c)** Object insertion into a virtual 3D scene. The red arrows indicate the objects relighted by *RelitLRM* using the scene illumination, demonstrating its ability to capture surrounding illumination and seamlessly harmonize with the scene background. **(d)** Objects relighting results showcase the robustness of our method under challenging lighting conditions, such as strong directional lighting. Our method faithfully models complex lighting effects, including removing shadow and highlights in input images and also casting strong shadows and glossy specular highlights under target lighting.

appearance, and illumination, resolving material-lighting ambiguities more effectively than prior models and enabling photorealistic rendering from novel viewpoints under novel lightings.

We conduct extensive experiments on synthetic and real-world datasets to evaluate RelitLRM. The results demonstrate that our method matches state-of-the-art inverse rendering approaches while using significantly fewer input images and requiring much less processing time (seconds v.s. hours). Additionally, RelitLRM does not rely on fixed analytic reflectance models, allowing greater flexibility in handling diverse material properties. Its scalability and efficiency make it well-suited for real-world applications where flexibility in lighting conditions and rapid processing are essential.

In summary, our key contributions to the field of relightable 3D reconstruction are:

- **Novel transformer-based generative relighting architecture.** We propose to use a regression-based geometry reconstructor followed by a diffusion-based appearance synthesizer (both modeled by transformers and trained end-to-end), to disentangle geometry from appearance, allowing better modeling of the uncertainty in relighting.

- **State-of-the-art performance with practical efficiency.** Trained on a large-scale 3D object dataset, RelitLRM matches or surpasses the performance of leading inverse rendering methods while using significantly fewer input images and less processing time, demonstrating superior generalization and practicality for real-world applications.

2 RELATED WORK

2.1 INVERSE RENDERING

Inverse rendering aims to recover intrinsic scene properties — geometry, material reflectance, and lighting — from images, enabling tasks like relighting and novel view synthesis. Traditional methods optimize through physically-based rendering equations (Kajiya, 1986) using dense image captures (typically 100–200 views) under controlled lighting (Debevec et al., 2000; Ramamoorthi & Hanrahan, 2001; Marschner, 1998). Propelled by the recent advances in Neural Radiance Fields (NeRF) (Mildenhall et al., 2020) and 3D Gaussian Splatting (3DGS) (Kerbl et al., 2023), recent learning-based inverse rendering methods have emerged to decompose the scene properties with

these neural representations (Bi et al., 2020b;a; Zhang et al., 2021a;b; Boss et al., 2021a;b; Luan et al., 2021; Srinivasan et al., 2021), by leveraging the differentiable rendering for their optimization and training (Boss et al., 2022; Zhang et al., 2022a;b; Kuang et al., 2022a;b; Jin et al., 2023; Shi et al., 2023; Yang et al., 2023; Zhang et al., 2023b; Gao et al., 2023; Liang et al., 2024; Jiang et al., 2024). However, these methods typically require dense inputs and computationally intensive optimization, limiting scalability and struggling with complex lighting and materials.

Our method addresses these challenges by efficiently reconstructing relightable 3D objects from sparse images (4–8 views) without per-scene optimization. Utilizing a transformer-based architecture integrated with neural implicit radiance representations within the 3DGS framework (Kerbl et al., 2023), we effectively disentangle geometry, appearance, and illumination, enabling high-quality relighting and rendering under unknown lighting conditions, surpassing previous methods in scalability and practicality.

2.2 LARGE RECONSTRUCTION MODEL

Advancements in 3D reconstruction have been driven by neural implicit representations like NeRF (Mildenhall et al., 2020) and 3DGS (Kerbl et al., 2023), enabling high-quality novel view synthesis. Built upon it, the Large Reconstruction Model (LRM) series has further enhanced 3D reconstruction using transformer-based architectures for feed-forward processing. Notable models such as Single-view LRM (Hong et al.), Instant3D (Li et al., 2023), DMV3D (Xu et al.), PF-LRM (Wang et al., 2023), and GS-LRM (Zhang et al., 2024a), along with others (Wei et al., 2024; Xie et al., 2024; Anciukevičius et al., 2023; Szymanowicz et al., 2023), have introduced scalable methods for multi-view data, enabling detailed reconstructions even from sparse inputs.

Despite these improvements, integrating relighting capabilities remains challenging. Our approach, RelitLRM, extends the LRM series by incorporating relightable reconstruction, combining transformer-based architecture with neural implicit radiance representations within the 3DGS framework. This enables robust 3D reconstruction with relighting capabilities from sparse inputs, overcoming scalability and practicality issues of previous methods.

2.3 IMAGE-BASED RELIGHTING AND DIFFUSION MODELS

Diffusion models have become prominent in visual content generation, excelling in tasks like text-to-image synthesis and image editing (Ho et al., 2020; Nichol & Dhariwal, 2021). Models such as Stable Diffusion (Rombach et al., 2022) and ControlNet (Zhang et al., 2023a) adapt diffusion frameworks for controlled image synthesis. While primarily 2D, recent works like Zero-1-to-3 (Liu et al., 2023) demonstrate diffusion models' latent understanding of 3D structures, relevant for view synthesis and relighting.

Single-image relighting is challenging due to the limited view of input data. Early neural network-based approaches (Ren et al., 2015; Xu et al., 2018) laid the groundwork, with recent portrait-focused methods (Sun et al., 2019; Zhou et al., 2019; Pandey et al., 2021; Mei et al., 2024; Ren et al., 2024) enhancing realism and lighting control. However, these methods are often domain-specific or rely on explicit scene decomposition, limiting adaptability. Recent methods like Neural Gaffer (Jin et al., 2024), DiLightNet (Zeng et al., 2024), and IC-Light (Zhang et al., 2024b) leverage diffusion models for precise lighting control, achieving high-quality relighting. However, All theses works are constrained to single-view inputs.

Our approach integrates generative relighting and 3D reconstruction into an end-to-end transformer-based architecture. It produce high-quality renderings of objects from novel viewpoints and under arbitrary lighting, given sparse input images.

3 METHOD

Our RelitLRM is built on top of the prior GS-LRM (Zhang et al., 2024a) model, but differs in crucial aspects: 1) we aim for relightability of the output assets; 2) to achieve this, we propose a novel generative relighting radiance component to replace GS-LRM's deterministic appearance part. In this section, we first briefly review the model architecture of GS-LRM, then describe in detail our relit 3D appearance generation algorithm based on relit-view diffusion.
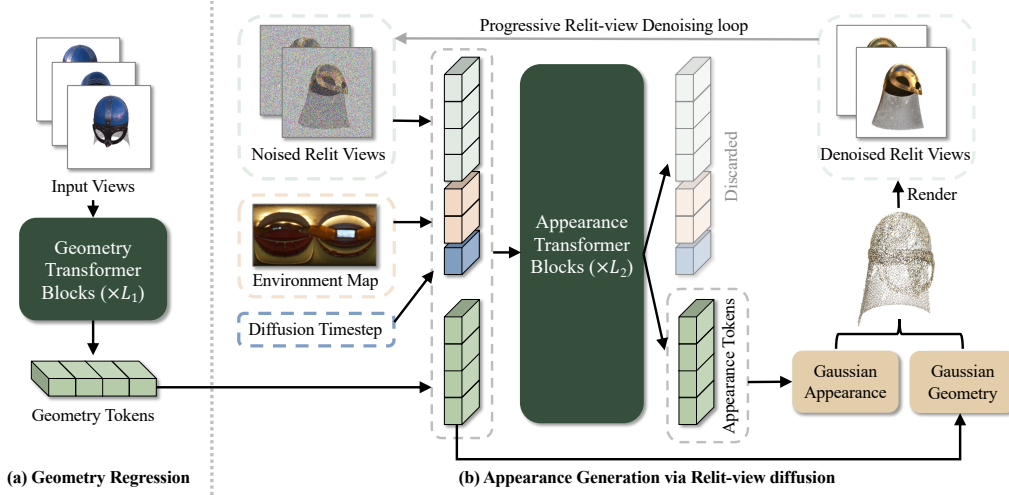
Figure 2: **Overview of *RelitLRM* for sparse-view relightable 3D reconstruction.** Our pipeline consists of a geometry regressor and a relit appearance generator, both implemented as transformer blocks and trained jointly end-to-end. We implicitly bake the relit appearance generation in relit-view diffusion process. During inference, we first extract geometry tokens from sparse input images and regress geometry parameters for per-pixel 3D Gaussians (3DGS). Conditioning on novel target lighting and extracted geometry features, we denoise the relit views by first predicting a 3DGS appearance, then render it (along with 3DGS geometry that stays fixed in the diffusion denoising loop) into the denoising viewpoints. This iterative process produces the relit 3DGS radiance as a byproduct while denoising the relit views. The generative appearance and deterministic geometry blocks are trained end-to-end, ensuring scalability.

3.1 REVIEW OF GS-LRM MODEL

GS-LRM (Zhang et al., 2024a) uses a transformer model for predicting 3DGS parameters from sparse posed images. They demonstrated instant photo-realistic 3D reconstruction results. We provide an overview of their method below.

Given a set of N images $I_i \in \mathcal{R}^{H \times W \times 3}, i = 1, 2, ..., N$ and corresponding camera Plücker rays $\mathbf{P}_i$, GS-LRM concatenates $I_i, \mathbf{P}_i$ channel-wise first, then converts the concatenated feature map into tokens using patch size p. The multi-view tokens are then processed by a sequence of L_1 transformer blocks for predicting 3DGS parameters $\mathbf{G}_{ij}$: one 3DGS at each input view pixel location.

$$\{\boldsymbol{T}_{ij}\}_{j=1,2,...,HW/p^2} = \text{Linear}\big(\text{Patchify}_p\big(\text{Concat}(I_i, \boldsymbol{P}_i)\big)\big), \tag{1}$$

$$\{\boldsymbol{T}_{ij}\}^0 = \{\boldsymbol{T}_{ij}\}, \tag{2}$$

$$\{\boldsymbol{T}_{ij}\}^l = \text{TransformerBlock}^l(\{\boldsymbol{T}_{ij}\}^{l-1}), \quad l = 1, 2, ..., L_1, \tag{3}$$

$$\{\mathbf{G}_{ij}\} = \text{Linear}(\{\boldsymbol{T}_{ij}\}^{L_1}). \tag{4}$$

The whole model is trained end-to-end using novel-view rendering loss on multi-view posed images.

3.2 GENERATING RELIT 3DGS APPEARANCE VIA RELIT VIEW DIFFUSION

The relighting procedure involves the removal of source lighting from input images, and relighting the objects under target lighting, which are inherently ambiguous in the case of sparse view observations and unknown lighting conditions, especially in regions of shadows and specularity. Moreover, when relighting glossy objects using high-frequency novel illuminations, the relit object appearance is inherently multi-modal with possibly many small specular regions; regression-based approaches tend to be dominated by large diffuse or weakly specular areas, ignoring the small strong specular highlights. Hence, to boost relighting quality, we need a generative model to better handle the uncertainty in relighting and multi-modality in relit radiance.

We design a new approach to generate relit 3DGS appearance under a novel lighting. Related to prior work (Xu et al.; Szymanowicz et al., 2023; Anciukevičius et al., 2023), we perform diffusion, in

which we force a 3D representation as a bottleneck. However, the key algorithmic innovation is that our appearance predictor is a relighting diffusion model, conditioned on the novel target illumination and the predicted geometry features. The relit-view denoiser uses x_0 prediction objective (Ramesh et al., 2022); at each denoising step, it outputs the denoised relit views by predicting and then rendering the relit 3D Gaussian representation.

Formally, we first predict 3DGS geometry parameters $\{\mathbf{G}_{ij}^{\text{geom}}\}$ using the same approach (see Eq. 1,2,3,4) as in GS-LRM (Zhang et al., 2024a); we also obtain the last transformer block's output $\{\boldsymbol{T}_{ij}^{\text{geom}}\}$ of this geometry network to use as input to our relit-view denoiser. To produce the relit 3DGS apperance under a target lighting, we then concatenate the noisy relit view tokens, target lighting tokens, denoising timestep token, and predicted 3DGS geometry tokens, passing them through a second transformer stack with L_2 layers. The process is described as follows:

$$\{\boldsymbol{T}_i^{\text{all}}\}^0 = \left\{ \{\boldsymbol{T}_{ij}^{\text{noised-relit-views}}\}^{L_1} \oplus \{\boldsymbol{T}_{ij}^{\text{light}}\} \oplus \{\boldsymbol{T}_{ij}^{\text{geom}}\} \oplus \{\boldsymbol{T}^{\text{timestep}}\} \right\}, \tag{5}$$

$$\{\boldsymbol{T}_i^{\text{all}}\}^l = \text{TransformerBlock}^{L_1+l}(\{\boldsymbol{T}_i^{\text{all}}\}^{l-1}), \quad l = 1, 2, \ldots, L_2. \tag{6}$$

The output tokens $\{\boldsymbol{T}_{ij}^{\text{geom}}\}^{L_2}$ are used to decode the appearance parameters of the 3D Gaussians, while the other tokens, e.g., $\{\boldsymbol{T}_{ij}^{\text{noised-relit-views}}\}^{L_2}$ are discarded on the output end. In detail, we predict the 3DGS spherical harmonics (SH) coefficients via a linear layer:

$$\{\boldsymbol{G}_{ij}^{\text{color}}\} = \text{Linear}\left(\{\boldsymbol{T}_{ij}^{\text{geom}}\}^{L_2}\right), \tag{7}$$

where $\boldsymbol{G}_{ij}^{\text{color}} \in \mathbb{R}^{75p^2}$ represents the 4-th order SH coefficients for the predicted per-pixel 3DGS in a pxp patch.

At each denoising step, we output the denoised relit views (using x_0 prediction objective) by rendering the predicted 3DGS representation:

$$\{\boldsymbol{I}_i^{\text{denoised-relit-views}}\} = \text{Render}\left(\{\boldsymbol{G}_{ij}^{\text{geom}}\}, \{\boldsymbol{G}_{ij}^{\text{color}}\}\right). \tag{8}$$

The interleaving of 3DGS appearance prediction and rendering in the relit-view denoising process allow us to generate a relit 3DGS appearance as a side product during inference time. We output the 3DGS at final denoising step as our model's final output: a 3DGS relit by target lighting.

Tokenizing HDR environment maps. To make it easier for networks to ingest HDR environment maps $E \in \mathcal{R}^{H_e \times W_e \times 3}$, we convert each E into two feature maps through two different tone-mappers: one E_1 emphasizing dark regions and one E_2 for bright regions. We then concatenate E_1, E_2 with the ray direction D, creating a 9-channel feature for each environment map pixel. Then we patchify it into light tokens, $\{\boldsymbol{T}_{ij}^{\text{light}}\}_{j=1,2,\ldots,H_eW_e/p_e^2}$, with a MLP. See Appendix 9 for details.

3.3 TRAINING SUPERVISION

In each training iteration, we sample a sparse set of input images for an object under a random lighting and another set of images of the same object under different lighting (along with its ground-truth environment map). The input posed images are first passed through the geometry transformer to extract object geometry features. As described in Sec. 3.2, we then perform relighting diffusion with the x_0 prediction objective; our denoiser is a transformer network translating predicted 3DGS geometry features into 3DGS appearance features, conditioning on the sampled novel lighting and noised multi-view images under this novel lighting (along with diffusion timestep).

We apply ℓ_2 and perceptual loss (Chen & Koltun, 2017) to the renderings at both the diffusion viewpoints and another two novel viewpoints in the same novel lighting. The deterministic geometry predictor and probabilistic relit view denoiser are trained jointly end-to-end from scratch.

3.4 SAMPLING RELIT RADIANCE

At inference time, we first reconstruct 3DGS geometry from the user-provided sparse images. Then we sample a relit radiance in the form of 3DGS spherical harmonics given a target illumination. Our relit radiance is implicitly generated by sampling the relit-view diffusion model. We use the DDIM sampler (Song et al., 2020) and classifier-free guidance technique (Ho & Salimans, 2022). Since the denoised relit views are rendered from the 3DGS geometry and predicted relit radiance at each denosing step, the relit-view denoising process also results in a chain of generated relit radiances. We only keep the relit radiance at last denoising step as our final predicted 3DGS appearance.

4 DATASET AND IMPLEMENTATION

Training dataset. Our training dataset is constructed from a combination of 800K objects sourced from Objaverse (Deitke et al., 2023) and 210K synthetic objects from Zeroverse (Xie et al., 2024). The inclusion of Zeroverse data, which features a higher proportion of concave objects, assists in training the model to handle complex shadowing effects. Additionally, We also modify the metallic properties and roughness of some Zeroverse objects to introduce more specular surfaces, adding variety and challenge to the dataset.

For lighting diversity, we gathered over 8,000 HDR environment maps from multiple sources, including Polyhaven[1], Laval Indoor (Gardner et al., 2017), Laval Outdoor (Hold-Geoffroy et al., 2019), internal datasets, and a selection of randomly generated Gaussian blobs. We augmented these maps with random horizontal rotations and flips, increasing their number 16-fold. Each object is rendered from 10 to 32 randomly selected viewpoints under 2 to 12 different lighting conditions.

Model details. Our model comprises 24 layers of transformer blocks for the geometry reconstruction stage and an additional 8 layers for the appearance diffusion (denoising) stage, with a hidden dimension of 1024 for the transformers and 4096 for the MLPs, totaling approximately 0.4 billion trainable parameters. We employ Pre-Layer Normalization (Xiong et al., 2020) and GeLU activations (Hendrycks & Gimpel, 2016).

Input images and environment maps are tokenized using an 8×8 patch size, while denoising views are tokenized with a 16×16 patch size to optimize computational efficiency. Tokenization is involves a simple reshape operation followed by a linear layer, with separate weights for the input and target image tokenizers. The diffusion timestep embedding is processed via an MLP similar to Peebles & Xie (2023), is appended to the input token set to the diffusion transformer.

Training details. The initial training phase employs four input views, four target denoising views (under target lighting, used for computing the diffusion loss), and two additional supervision views (under target lighting), all at a resolution of 256×256, with the environment map set to 128×256. The model is trained with a batch size of 512 for 80K iterations, introducing the perceptual loss after the first 5K iterations to enhance training stability. Following this pretraining at the 256-resolution, we fine-tune the model for a larger context by increasing to six input views and six denosing target views at a higher resolution of 512×512. This fine-tuning expands the context window to up to 31K tokens. For diffusion training, we discretize the noise into 1,000 timesteps, adhering to the method described in Ho et al. (2020), with a variance schedule that linearly increases from 0.00085 to 0.0120. To enable classifier-free guidance, environment map tokens are randomly masked to zero with a probability of 0.1 during training. For more details, please refer to Appendix.

Sampling details. We performed an ablation study on the key hyperparameters, specifically the number of denoising steps and the classifier-free guidance (CFG) weight, as detailed in Table 6. We found our model can produce realistic and diverse results with five sampling steps, and CFG of 3.0 gives the best result for our res-256 model.

5 EXPERIMENTS

We refer the readers to our project page for video results and interactive visualizations.

5.1 COMPARISON WITH OPTIMIZATION-BASED METHODS

Current optimization-based inverse rendering algorithms achieve state-of-the-art 3D relighting results, but typically require dense view captures (over 40 views) and long optimization times, often taking several hours, using traditional rendering techniques like rasterization, path tracing, or neural rendering.

We evaluate our method against these approaches on three publicly available datasets: STANFORD-ORB (Kuang et al., 2024), OBJECTS-WITH-LIGHTING (Ummenhofer et al., 2024), and TENSOIR-
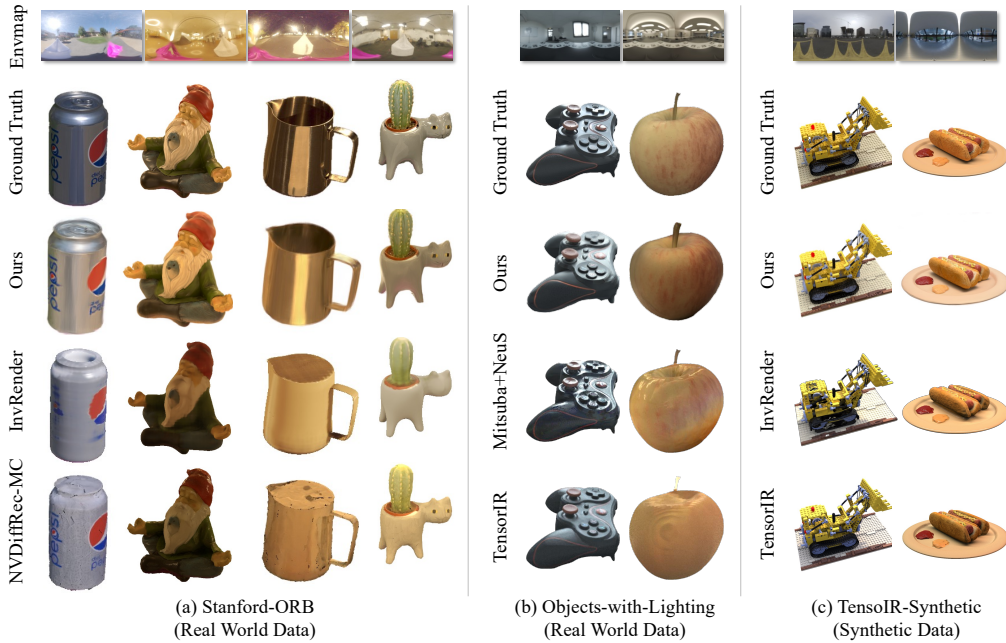
---

[1]https://polyhaven.com/hdris

Figure 3: **Comparison with optimization-based inverse rendering baselines** on STANFORD-ORB (Kuang et al., 2024), OBJECTS-WITH-LIGHTING (Ummenhofer et al., 2024), and TENSOIR-SYNTHETIC (Jin et al., 2023) datasets. (a) On STANFORD-ORB, our method captures realistic specular highlights and geometric details, outperforming NVDiffRec-MC(Hasselgren et al., 2022) and InvRender (Zhang et al., 2022b). (b) On OBJECTS-WITH-LIGHTING, our results closely match the ground truth, while baselines show over-specularity or artifacts. (c) For TENSOIR-SYNTHETIC, our method achieves comparable relighting with significantly fewer views. Notably, our method requires only 6 to 8 views and completes relighting in 2-3 seconds, while baselines need over 50 views and hours of processing.

SYNTHETIC (Jin et al., 2023). The STANFORD-ORB dataset comprises 14 objects captured under three lighting conditions, with 60 training views and 10 test views per lighting setup. The OBJECTS-WITH-LIGHTING dataset contains 7 objects with dense views captured under one training lighting condition and 3 views for two additional lighting conditions for testing. The TENSOIR-SYNTHETIC dataset consists of 4 objects with 100 training views under one lighting condition and 200 test views for each of five lighting conditions.

Our method requires only **six input views** for STANFORD-ORB and OBJECTS-WITH-LIGHTING and **eight input views** for TENSOIR-SYNTHETIC, completing the entire reconstruction and relighting process in just **2 to 3 seconds**. In contrast, state-of-the-art optimization-based methods typically rely on all available training views (60 views per object for STANFORD-ORB, 42-67 views per object for OBJECTS-WITH-LIGHTING, and 100 views per object for TENSOIR-SYNTHETIC) and take several hours to optimize. Despite using significantly fewer input views and processing time, our method achieves comparable reconstruction and relighting results, as demonstrated in Table 1 and Table 2, showcasing its remarkable efficiency. Qualitative comparisons in Figure 3 further highlight our method's superior performance across various scenarios. Optimization-based methods struggle with high uncertainties when decomposing object appearances under input lighting and relighting, leading to baked highlights (Column-6 in Figure 3) and poor specular reflections (Columns 1 and 3). In contrast, our generative approach handles these challenges effectively.

5.2 COMPARISON WITH DATA-DRIVEN BASED RELIGHTING METHODS

We also compare our method with state-of-the-art image relighting approaches (Jin et al., 2024; Zeng et al., 2024), which fine-tune text-to-image diffusion models for single-image relighting. These methods, however, only support relighting from the input views and do not handle novel view re-

Table 1: **Real world experiments**. We compare our method with state-of-the-art optimization-based approaches on the STANFORD-ORB (Kuang et al., 2024) and OBJECTS-WITH-LIGHTING (Ummenhofer et al., 2024) datasets. Our method offers competitive relighting results, but uses only six input views and runs within seconds on a single A100 GPU, whereas other methods require 60 views for STANFORD-ORB and 42 to 67 views for Objects-With-Lighting, taking hours to complete.

| Method | STANFORD-ORB | | | | OBJECTS-WITH-LIGHTING | | | # Input views | Runtime |
	PSNR-H ↑	PSNR-L ↑	SSIM ↑	LPIPS ↓	PSNR ↑	SSIM ↑	LPIPS ↓		
Ours	24.67	31.52	0.969	0.032	23.08	0.79	0.284	6	∼2 seconds
Neural-PBIR	26.01	33.26	0.979	0.023	N/A	N/A	N/A	42-67	hours
Mitsuba+Neus	N/A	N/A	N/A	N/A	26.24	0.84	0.227	42-67	hours
NVDIFFREC-MC	24.43	31.60	0.972	0.036	20.24	0.73	0.393	42-67	hours
InvRender	23.76	30.83	0.970	0.046	23.45	0.77	0.374	42-67	hours
TensoIR	N/A	N/A	N/A	N/A	24.15	0.77	0.378	42-67	hours
NeRFactor	23.54	30.38	0.969	0.048	20.62	0.72	0.486	42-67	hours
NVDIFFREC	22.91	29.72	0.963	0.039	22.60	0.72	0.406	42-67	hours
PhySG	21.81	28.11	0.960	0.055	22.77	0.82	0.375	42-67	hours

Table 2: **Comparison with dense-view optimization-based methods on TensoIR-Synthetic.** This dataset from (Jin et al., 2023) includes 4 scenes, each having 100 training views and 5 lighting conditions with 200 test views. We report per-scene and average metrics. Baselines use 100 input views; our method uses only eight. * indicates rescaling in pixel space instead of albedo.

| Method | Armadillo | | Ficus | | Hotdog | | Lego | | Average | | | # Input views | Runtime |
	PSNR	SSIM	PSNR	SSIM	PSNR	SSIM	PSNR	SSIM	PSNR	SSIM	LPIPS		
Ours*	33.25	0.966	26.18	0.952	29.32	0.938	27.44	0.886	29.05	0.936	0.082	8	∼3 second
FlashCache	34.81	0.959	26.29	0.960	29.24	0.941	28.56	0.917	29.72	0.944	0.080	100	hours
TensoIR*	34.75	0.974	25.66	0.950	28.78	0.932	29.37	0.932	29.64	0.947	0.068	100	hours
TensoIR	34.50	0.975	24.30	0.947	27.93	0.933	27.60	0.922	28.58	0.944	0.081	100	hours
InvRender	27.81	0.949	20.33	0.895	27.63	0.928	20.12	0.832	23.97	0.901	0.101	100	hours
NeRFactor	26.89	0.944	20.68	0.907	22.71	0.914	23.25	0.865	23.38	0.908	0.131	100	hours

lighting. Real-world benchmarks like STANFORD-ORB and OBJECTS-WITH-LIGHTING focus on novel view relighting, making these methods unsuitable for direct evaluation on those datasets.

To ensure a fair comparison, we construct a held-out set from filtered Objaverse (unseen during training), comprising 7 highly specular objects and 6 concave objects with shadows. Each object is rendered under five environment maps with four viewpoints, resulting in a total of 260 images for evaluation. We compute PSNR, SSIM, and LPIPS metrics, after applying per-channel RGB scaling to align predictions with the ground truth, following (Jin et al., 2024). Our method outperforms the baselines, showing better image quality metrics as in Table 3.

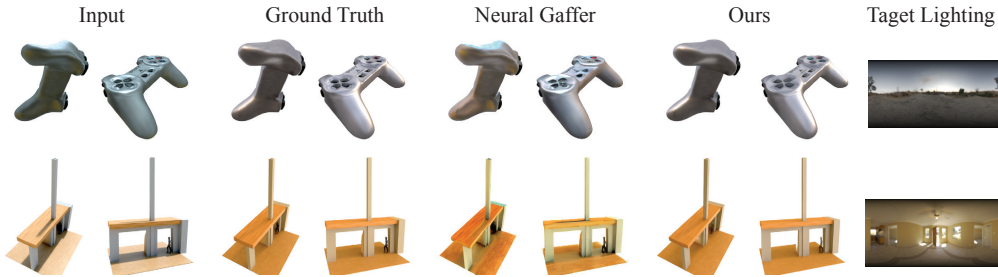| Input | Ground Truth | Neural Gaffer | Ours | Taget Lighting |

Figure 4: **Comparison with image-based relighting baseline** on our held-out evaluation set shows that our model produces better visual quality, with improved shadow removal and highlight. Our model processes four input images jointly, while the baseline relights each image independently.

5.3 OBJECT SCENE INSERTION

RelitLRM's capability to accurately reconstruct and relight 3D objects makes it particularly effective for object scene insertion tasks, where the goal is to seamlessly integrate objects into existing environments, as demonstrated in Fig. 1(c) and Fig. 1(d). In Fig. 1(c), we demonstrate the insertion of two objects into an indoor living-room scene, where they harmonize naturally with the surrounding lighting and shadows. In Fig. 1(d), we present that eight objects are relit under strong directional sunlight with our method, showcasing their ability to cast realistic shadows and exhibit
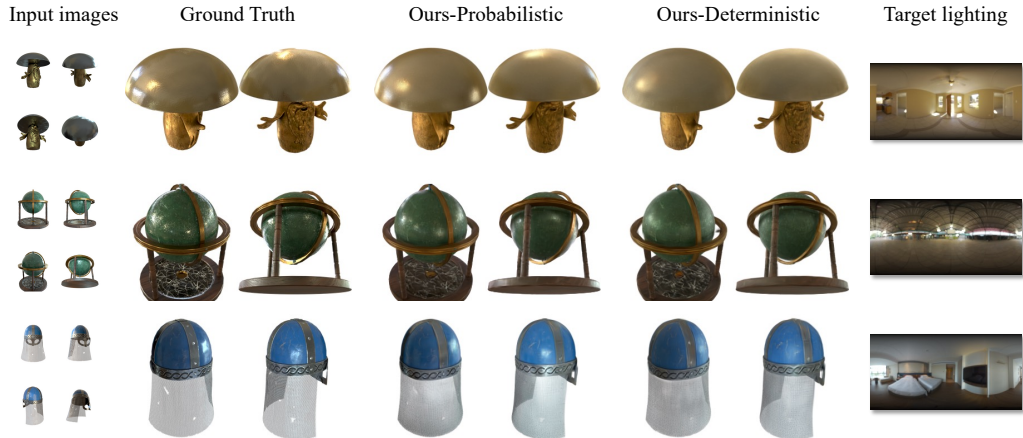
Figure 5: **Our probabilistic design yields significantly better results on specular highlights compared to the deterministic counterpart.** The radiance function of specular objects under challenging lighting is highly multi-modal with long tails. Our denoising diffusion approach models this distribution more effectively, while the deterministic design fails to mode such complex distribution and produce overly smooth specular highlights.

Table 3: **Comparison with image-based relighting models on held-out validation set.** The prediction is scaled per-channel to align with the target following (Jin et al., 2024). The PSNR is only computed in masked foreground regions. Our method takes four input views, and baseline methods take each view independently.

	PSNR ↑	SSIM ↑	LPIPS ↓	NFE	Parameters
Ours	**28.50**	**0.93**	**0.058**	5	0.4B
NeuralGaffer	24.51	0.90	0.072	50	0.9B
DiLightNet	20.02	0.85	0.132	20	0.9B

Table 4: **Ablation on probabilistic design**. We design a deterministic counterpart by removing the noisy image tokens and keeping the model architecture and training configuration the same. We compare our probabilistic design with the deterministic counterpart on held-out evaluation set. See Figure 5 for visual results.

	Input Views	PSNR ↑	SSIM ↑	LPIPS ↓
Ours-Probabilistic	4	27.63	0.922	0.064
Ours-Deterministic	4	27.10	0.912	0.076

accurate specular highlights, demonstrating RelitLRM's effectiveness in handling diverse lighting conditions.

5.4 ABLATION STUDY

Deterministic vs. probabilistic relighting. Decomposing object's appearance from input lighting and relighting is inherently ambiguous. Moreover, the radiance function of object under high-frequency lighting is extremely complex and highly multi-modal, e.g. containing multiple small sharp highlights. To address this, our model reconstructs geometry deterministically while relighting the object's radiance probabilistically using a diffusion approach. To evaluate this design, we introduce a deterministic baseline that relights objects directly, without the diffusion step, using the same architecture, amount of parameters, and training iterations. We assess both models on our hold-out validation set, with metrics presented in Table 4 and visual comparisons in Fig. 5. Although the quantitative results are similar, the probabilistic approach significantly improves visual quality for specular objects. This supports the idea that our probabilistic design captures the complex multi-modal radiance function more effectively than the deterministic counterpart, which tends to produce over-smooth results.

Effects of more input views. We evaluate our model with gradually increased number of input images up to 16 (70K input tokens) on our held-out set and TensoIR-Synthetic as shown in Table 5. We observe a positive correlation between our relighting quality and the number of input images.

Table 5: **Impact of more input views**: We evaluate the Res-512 model by incrementally adding more input views and compare its performance on our hold-out evaluation set and TENSOIR-SYNTHETIC. The Res-512 model is fine-tuned from the Res-256 model using six input views and six denoising views, and fixed through this evaluation.

HOLDOUT VALIDATION SET				TENSOIR-SYNTHETIC			
Input Views	PSNR ↑	SSIM ↑	LPIPS ↓	Input Views	PSNR ↑	SSIM ↑	LPIPS ↓
2	23.58	0.896	0.113	4	27.83	0.926	0.091
4	26.14	0.915	0.086	8	29.04	0.936	0.082
6	27.71	0.926	0.072	12	29.27	0.938	0.081
8	28.08	0.929	0.070	16	29.31	0.938	0.080

Table 6: **Ablation on the parameter space of diffusion** with four input views at 256×256 resolution in our holdout evaluation set. Default setting is marked as gray.

(a) **Number of denoising views**.

views	PSNR ↑	SSIM ↑	LPIPS ↓
1	27.05	0.913	0.075
2	26.87	0.913	0.0745
4	27.63	0.922	0.064

(b) **Classifier-free guidance**.

CFG	PSNR ↑	SSIM ↑	LPIPS ↓
1.0	27.00	0.915	0.072
3.0	27.63	0.922	0.064
6.0	23.64	0.891	0.0974

(c) **Number of denoising steps**.

steps	PSNR ↑	SSIM ↑	LPIPS ↓
2	23.81	0.884	0.096
5	27.63	0.922	0.064
10	27.00	0.915	0.073

Hyper-parameters in diffusion. In our model, the number of denoising views is independent of the number of input views. After all denoising steps, the virtual denoising views are discard, leaving only the 3D Gaussians for relighting at arbitrary views. A key question is how the denoising views affect the results. Additionally, two other parameters significantly impact relighting performance: the classifier free guidance weight and number of denoising steps. We present qualitative ablation results in Table 6. For classifier-free guidance, we visualize its effect in Fig. 6, where the unconditional predictions looks like relighting under average lighting in our dataset, and higher CFG weights making the object appear more specular.
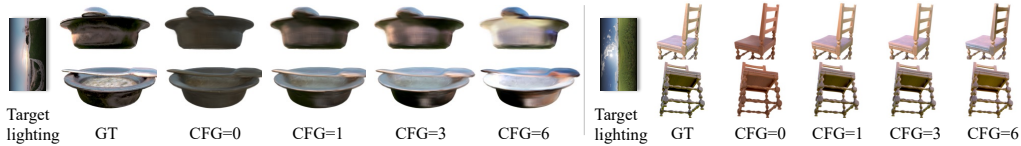

Figure 6: **Effect of classifier-free-guidance (CFG).** We show two novel-view relighting results with different CFG weight. Zero weight denotes unconditional relighting, which resembles relighting with average dataset lighting. Higher CFG weight makes the object more specular.

5.5 LIMITATIONS

Despite our model reconstructs and relights objects from sparse-view images, it requires camera parameters for the input views, which can be impractical in some cases. Although the model improves output quality with more input images, performance saturates around 16 views (as shown in Table 5). Improving scalability with additional input views and higher resolutions remains an area for future exploration. Additionally, our model uses environment maps as the target lighting representation, which cannot accurately represent near-field lighting.

6 CONCLUSION

In this paper, we introduced RelitLRM, a generative Large Reconstruction Model that reconstructs high-quality, relightable 3D objects from sparse input images using a transformer-based architecture. Our model disentangles geometry and appearance modeling, and uses a deterministic geometry reconstructor followed by a probabilistic appearance (in the form of radiance) generator based on relit-view diffusion. Trained on massive relighting datasets, RelitLRM effectively captures complex lighting effects like shadows, specularity, etc; it not only matches but also often exceeds state-of-the-art baselines while requiring significantly fewer input images and achieves this in just 2 to 3 seconds,

compared to the hours needed by per-scene optimization methods. This highlights its remarkable efficiency and potential for real-world applications in relightable 3D reconstruction.

Ethics Statement. This work proposes a large reconstruction model with a generative relightable radiance component, which can be used to reconstruct relightable 3D assets from sparse images. The proposed model tries best to preserve the identity of objects in the captured images in the reconstruction process; hence it might be used for reconstructing 3D from images with humans or commerical IPs.

Reproducibility Statement. We have included enough details in this main paper (Sec. 4) and appendix (Sec. A.1) to ensure reproducibility, which includes our training and testing data, model architecture, training setup, etc. We are also happy to address any questions regarding the implementation details of our paper, if any.

REFERENCES

Titas Anciukevičius, Zexiang Xu, Matthew Fisher, Paul Henderson, Hakan Bilen, Niloy J Mitra, and Paul Guerrero. Renderdiffusion: Image diffusion for 3d reconstruction, inpainting and generation. In *Proceedings of the IEEE/CVF conference on computer vision and pattern recognition*, pp. 12608–12618, 2023.

Sai Bi, Zexiang Xu, Pratul Srinivasan, Ben Mildenhall, Kalyan Sunkavalli, Miloš Hašan, Yannick Hold-Geoffroy, David Kriegman, and Ravi Ramamoorthi. Neural reflectance fields for appearance acquisition. *arXiv preprint arXiv:2008.03824*, 2020a.

Sai Bi, Zexiang Xu, Kalyan Sunkavalli, Miloš Hašan, Yannick Hold-Geoffroy, David Kriegman, and Ravi Ramamoorthi. Deep reflectance volumes: Relightable reconstructions from multi-view photometric images. In *Computer Vision–ECCV 2020: 16th European Conference, Glasgow, UK, August 23–28, 2020, Proceedings, Part III 16*, pp. 294–311. Springer, 2020b.

Mark Boss, Raphael Braun, Varun Jampani, Jonathan T Barron, Ce Liu, and Hendrik Lensch. Nerd: Neural reflectance decomposition from image collections. In *Proceedings of the IEEE/CVF International Conference on Computer Vision*, pp. 12684–12694, 2021a.

Mark Boss, Varun Jampani, Raphael Braun, Ce Liu, Jonathan Barron, and Hendrik Lensch. Neural-pil: Neural pre-integrated lighting for reflectance decomposition. *Advances in Neural Information Processing Systems*, 34:10691–10704, 2021b.

Mark Boss, Andreas Engelhardt, Abhishek Kar, Yuanzhen Li, Deqing Sun, Jonathan Barron, Hendrik Lensch, and Varun Jampani. Samurai: Shape and material from unconstrained real-world arbitrary image collections. *Advances in Neural Information Processing Systems*, 35:26389–26403, 2022.

Qifeng Chen and Vladlen Koltun. Photographic image synthesis with cascaded refinement networks. In *Proceedings of the IEEE international conference on computer vision*, pp. 1511–1520, 2017.

Paul Debevec, Tim Hawkins, Chris Tchou, Haarm-Pieter Duiker, Westley Sarokin, and Mark Sagar. Acquiring the reflectance field of a human face. In *Proceedings of the 27th annual conference on Computer graphics and interactive techniques*, pp. 145–156, 2000.

Matt Deitke, Dustin Schwenk, Jordi Salvador, Luca Weihs, Oscar Michel, Eli VanderBilt, Ludwig Schmidt, Kiana Ehsani, Aniruddha Kembhavi, and Ali Farhadi. Objaverse: A universe of annotated 3d objects. In *Proceedings of the IEEE/CVF Conference on Computer Vision and Pattern Recognition*, pp. 13142–13153, 2023.

Jian Gao, Chun Gu, Youtian Lin, Hao Zhu, Xun Cao, Li Zhang, and Yao Yao. Relightable 3d gaussian: Real-time point cloud relighting with brdf decomposition and ray tracing. *arXiv preprint arXiv:2311.16043*, 2023.

Marc-André Gardner, Kalyan Sunkavalli, Ersin Yumer, Xiaohui Shen, Emiliano Gambaretto, Christian Gagné, and Jean-François Lalonde. Learning to predict indoor illumination from a single image. *arXiv preprint arXiv:1704.00090*, 2017.

Jon Hasselgren, Nikolai Hofmann, and Jacob Munkberg. Shape, light, and material decomposition from images using monte carlo rendering and denoising. *Advances in Neural Information Processing Systems*, 35:22856–22869, 2022.

Dan Hendrycks and Kevin Gimpel. Gaussian error linear units (gelus). *arXiv preprint arXiv:1606.08415*, 2016.

Jonathan Ho and Tim Salimans. Classifier-free diffusion guidance. *arXiv preprint arXiv:2207.12598*, 2022.

Jonathan Ho, Ajay Jain, and Pieter Abbeel. Denoising diffusion probabilistic models. *Advances in neural information processing systems*, 33:6840–6851, 2020.

Yannick Hold-Geoffroy, Akshaya Athawale, and Jean-François Lalonde. Deep sky modeling for single image outdoor lighting estimation. In *Proceedings of the IEEE/CVF conference on computer vision and pattern recognition*, pp. 6927–6935, 2019.

Yicong Hong, Kai Zhang, Jiuxiang Gu, Sai Bi, Yang Zhou, Difan Liu, Feng Liu, Kalyan Sunkavalli, Trung Bui, and Hao Tan. Lrm: Large reconstruction model for single image to 3d.

Yingwenqi Jiang, Jiadong Tu, Yuan Liu, Xifeng Gao, Xiaoxiao Long, Wenping Wang, and Yuexin Ma. Gaussianshader: 3d gaussian splatting with shading functions for reflective surfaces. In *Proceedings of the IEEE/CVF Conference on Computer Vision and Pattern Recognition*, pp. 5322–5332, 2024.

Haian Jin, Isabella Liu, Peijia Xu, Xiaoshuai Zhang, Songfang Han, Sai Bi, Xiaowei Zhou, Zexiang Xu, and Hao Su. Tensoir: Tensorial inverse rendering. In *Proceedings of the IEEE/CVF Conference on Computer Vision and Pattern Recognition*, pp. 165–174, 2023.

Haian Jin, Yuan Li, Fujun Luan, Yuanbo Xiangli, Sai Bi, Kai Zhang, Zexiang Xu, Jin Sun, and Noah Snavely. Neural gaffer: Relighting any object via diffusion. *arXiv preprint arXiv:2406.07520*, 2024.

James T Kajiya. The rendering equation. In *Proceedings of the 13th annual conference on Computer graphics and interactive techniques*, pp. 143–150, 1986.

Bernhard Kerbl, Georgios Kopanas, Thomas Leimkühler, and George Drettakis. 3d gaussian splatting for real-time radiance field rendering. *ACM Trans. Graph.*, 42(4):139–1, 2023.

Zhengfei Kuang, Fujun Luan, Sai Bi, Zhixin Shu, Gordon Wetzstein, and Kalyan Sunkavalli. Palettenerf: Palette-based appearance editing of neural radiance fields. *arXiv preprint arXiv:2212.10699*, 2022a.

Zhengfei Kuang, Kyle Olszewski, Menglei Chai, Zeng Huang, Panos Achlioptas, and Sergey Tulyakov. Neroic: Neural rendering of objects from online image collections. *ACM Transactions on Graphics (TOG)*, 41(4):1–12, 2022b.

Zhengfei Kuang, Yunzhi Zhang, Hong-Xing Yu, Samir Agarwala, Elliott Wu, Jiajun Wu, et al. Stanford-orb: a real-world 3d object inverse rendering benchmark. *Advances in Neural Information Processing Systems*, 36, 2024.

Jiahao Li, Hao Tan, Kai Zhang, Zexiang Xu, Fujun Luan, Yinghao Xu, Yicong Hong, Kalyan Sunkavalli, Greg Shakhnarovich, and Sai Bi. Instant3d: Fast text-to-3d with sparse-view generation and large reconstruction model. *arXiv preprint arXiv:2311.06214*, 2023.

Zhihao Liang, Qi Zhang, Ying Feng, Ying Shan, and Kui Jia. Gs-ir: 3d gaussian splatting for inverse rendering. In *Proceedings of the IEEE/CVF Conference on Computer Vision and Pattern Recognition*, pp. 21644–21653, 2024.

Ruoshi Liu, Rundi Wu, Basile Van Hoorick, Pavel Tokmakov, Sergey Zakharov, and Carl Vondrick. Zero-1-to-3: Zero-shot one image to 3d object. In *Proceedings of the IEEE/CVF international conference on computer vision*, pp. 9298–9309, 2023.

Fujun Luan, Shuang Zhao, Kavita Bala, and Zhao Dong. Unified shape and svbrdf recovery using differentiable monte carlo rendering. In *Computer Graphics Forum*, volume 40, pp. 101–113. Wiley Online Library, 2021.

Stephen Robert Marschner. *Inverse rendering for computer graphics*. Cornell University, 1998.

Yiqun Mei, Yu Zeng, He Zhang, Zhixin Shu, Xuaner Zhang, Sai Bi, Jianming Zhang, HyunJoon Jung, and Vishal M. Patel. Holo-relighting: Controllable volumetric portrait relighting from a single image. In *Proceedings of the IEEE/CVF Conference on Computer Vision and Pattern Recognition (CVPR)*, pp. 4263–4273, June 2024.

Ben Mildenhall, Pratul P. Srinivasan, Matthew Tancik, Jonathan T. Barron, Ravi Ramamoorthi, and Ren Ng. Nerf: Representing scenes as neural radiance fields for view synthesis. In *ECCV*, 2020.

Alexander Quinn Nichol and Prafulla Dhariwal. Improved denoising diffusion probabilistic models. In *International conference on machine learning*, pp. 8162–8171. PMLR, 2021.

Rohit Pandey, Sergio Orts-Escolano, Chloe Legendre, Christian Haene, Sofien Bouaziz, Christoph Rhemann, Paul E Debevec, and Sean Ryan Fanello. Total relighting: learning to relight portraits for background replacement. *ACM Trans. Graph.*, 40(4):43–1, 2021.

William Peebles and Saining Xie. Scalable diffusion models with transformers. In *Proceedings of the IEEE/CVF International Conference on Computer Vision*, pp. 4195–4205, 2023.

Ravi Ramamoorthi and Pat Hanrahan. A signal-processing framework for inverse rendering. In *Proceedings of the 28th annual conference on Computer graphics and interactive techniques*, pp. 117–128, 2001.

Aditya Ramesh, Prafulla Dhariwal, Alex Nichol, Casey Chu, and Mark Chen. Hierarchical text-conditional image generation with clip latents. *arXiv preprint arXiv:2204.06125*, 1(2):3, 2022.

Mengwei Ren, Wei Xiong, Jae Shin Yoon, Zhixin Shu, Jianming Zhang, HyunJoon Jung, Guido Gerig, and He Zhang. Relightful harmonization: Lighting-aware portrait background replacement. In *Proceedings of the IEEE/CVF Conference on Computer Vision and Pattern Recognition*, pp. 6452–6462, 2024.

Peiran Ren, Yue Dong, Stephen Lin, Xin Tong, and Baining Guo. Image based relighting using neural networks. *ACM Transactions on Graphics (ToG)*, 34(4):1–12, 2015.

Robin Rombach, Andreas Blattmann, Dominik Lorenz, Patrick Esser, and Björn Ommer. High-resolution image synthesis with latent diffusion models. In *Proceedings of the IEEE/CVF conference on computer vision and pattern recognition*, pp. 10684–10695, 2022.

Yahao Shi, Yanmin Wu, Chenming Wu, Xing Liu, Chen Zhao, Haocheng Feng, Jingtuo Liu, Liangjun Zhang, Jian Zhang, Bin Zhou, et al. Gir: 3d gaussian inverse rendering for relightable scene factorization. *arXiv preprint arXiv:2312.05133*, 2023.

Jiaming Song, Chenlin Meng, and Stefano Ermon. Denoising diffusion implicit models. *arXiv preprint arXiv:2010.02502*, 2020.

Pratul P Srinivasan, Boyang Deng, Xiuming Zhang, Matthew Tancik, Ben Mildenhall, and Jonathan T Barron. Nerv: Neural reflectance and visibility fields for relighting and view synthesis. In *Proceedings of the IEEE/CVF Conference on Computer Vision and Pattern Recognition*, pp. 7495–7504, 2021.

Tiancheng Sun, Jonathan T Barron, Yun-Ta Tsai, Zexiang Xu, Xueming Yu, Graham Fyffe, Christoph Rhemann, Jay Busch, Paul Debevec, and Ravi Ramamoorthi. Single image portrait relighting. *ACM Transactions on Graphics (TOG)*, 38(4):1–12, 2019.

Stanislaw Szymanowicz, Christian Rupprecht, and Andrea Vedaldi. Viewset diffusion:(0-) image-conditioned 3d generative models from 2d data. In *Proceedings of the IEEE/CVF International Conference on Computer Vision*, pp. 8863–8873, 2023.

Benjamin Ummenhofer, Sanskar Agrawal, Rene Sepulveda, Yixing Lao, Kai Zhang, Tianhang Cheng, Stephan Richter, Shenlong Wang, and German Ros. Objects with lighting: A real-world dataset for evaluating reconstruction and rendering for object relighting. In *2024 International Conference on 3D Vision (3DV)*, pp. 137–147. IEEE, 2024.

Peng Wang, Hao Tan, Sai Bi, Yinghao Xu, Fujun Luan, Kalyan Sunkavalli, Wenping Wang, Zexiang Xu, and Kai Zhang. Pf-lrm: Pose-free large reconstruction model for joint pose and shape prediction. *arXiv preprint arXiv:2311.12024*, 2023.

Xinyue Wei, Kai Zhang, Sai Bi, Hao Tan, Fujun Luan, Valentin Deschaintre, Kalyan Sunkavalli, Hao Su, and Zexiang Xu. Meshlrm: Large reconstruction model for high-quality mesh. *arXiv preprint arXiv:2404.12385*, 2024.

Desai Xie, Sai Bi, Zhixin Shu, Kai Zhang, Zexiang Xu, Yi Zhou, Sören Pirk, Arie Kaufman, Xin Sun, and Hao Tan. Lrm-zero: Training large reconstruction models with synthesized data. *arXiv preprint arXiv:2406.09371*, 2024.

Ruibin Xiong, Yunchang Yang, Di He, Kai Zheng, Shuxin Zheng, Chen Xing, Huishuai Zhang, Yanyan Lan, Liwei Wang, and Tieyan Liu. On layer normalization in the transformer architecture. In *International Conference on Machine Learning*, pp. 10524–10533. PMLR, 2020.

Yinghao Xu, Hao Tan, Fujun Luan, Sai Bi, Peng Wang, Jiahao Li, Zifan Shi, Kalyan Sunkavalli, Gordon Wetzstein, Zexiang Xu, et al. Dmv3d: Denoising multi-view diffusion using 3d large reconstruction model. In *The Twelfth International Conference on Learning Representations*.

Zexiang Xu, Kalyan Sunkavalli, Sunil Hadap, and Ravi Ramamoorthi. Deep image-based relighting from optimal sparse samples. *ACM Transactions on Graphics (ToG)*, 37(4):1–13, 2018.

Ziyi Yang, Yanzhen Chen, Xinyu Gao, Yazhen Yuan, Yu Wu, Xiaowei Zhou, and Xiaogang Jin. Sire-ir: Inverse rendering for brdf reconstruction with shadow and illumination removal in high-illuminance scenes. *arXiv preprint arXiv:2310.13030*, 2023.

Chong Zeng, Yue Dong, Pieter Peers, Youkang Kong, Hongzhi Wu, and Xin Tong. Dilightnet: Fine-grained lighting control for diffusion-based image generation. In *ACM SIGGRAPH 2024 Conference Papers*, pp. 1–12, 2024.

Kai Zhang, Fujun Luan, Qianqian Wang, Kavita Bala, and Noah Snavely. Physg: Inverse rendering with spherical gaussians for physics-based material editing and relighting. In *Proceedings of the IEEE/CVF Conference on Computer Vision and Pattern Recognition*, pp. 5453–5462, 2021a.

Kai Zhang, Fujun Luan, Zhengqi Li, and Noah Snavely. Iron: Inverse rendering by optimizing neural sdfs and materials from photometric images. In *Proceedings of the IEEE/CVF Conference on Computer Vision and Pattern Recognition*, pp. 5565–5574, 2022a.

Kai Zhang, Sai Bi, Hao Tan, Yuanbo Xiangli, Nanxuan Zhao, Kalyan Sunkavalli, and Zexiang Xu. Gs-lrm: Large reconstruction model for 3d gaussian splatting. *arXiv preprint arXiv:2404.19702*, 2024a.

Lvmin Zhang, Anyi Rao, and Maneesh Agrawala. Adding conditional control to text-to-image diffusion models. In *Proceedings of the IEEE/CVF International Conference on Computer Vision*, pp. 3836–3847, 2023a.

Lvmin Zhang, Anyi Rao, and Maneesh Agrawala. Ic-light github page, 2024b.

Xiuming Zhang, Pratul P Srinivasan, Boyang Deng, Paul Debevec, William T Freeman, and Jonathan T Barron. Nerfactor: Neural factorization of shape and reflectance under an unknown illumination. *ACM Transactions on Graphics (ToG)*, 40(6):1–18, 2021b.

Youjia Zhang, Teng Xu, Junqing Yu, Yuteng Ye, Yanqing Jing, Junle Wang, Jingyi Yu, and Wei Yang. Nemf: Inverse volume rendering with neural microflake field. In *Proceedings of the IEEE/CVF International Conference on Computer Vision*, pp. 22919–22929, 2023b.

Yuanqing Zhang, Jiaming Sun, Xingyi He, Huan Fu, Rongfei Jia, and Xiaowei Zhou. Modeling indirect illumination for inverse rendering. In *Proceedings of the IEEE/CVF Conference on Computer Vision and Pattern Recognition*, pp. 18643–18652, 2022b.

Hao Zhou, Sunil Hadap, Kalyan Sunkavalli, and David W Jacobs. Deep single-image portrait relighting. In *Proceedings of the IEEE/CVF international conference on computer vision*, pp. 7194–7202, 2019.

A APPENDIX

A.1 PSEUDO CODE

Algorithm 1 RelitLRM pseudo code.

```
# one training iter of RelitLRM
# Input list:
# x_inp: [b, n, h, w, 3], n is number of views; h and w are the height and width;
# x_inp_ray_o, x_inp_ray_d: both [b, n, h, w, 3]. per-pixel ray direction and ray
      origins for input images.
# target_relit_image: [b, n1, h, w, 3], n1 is the number of denosing views.
# extra_train_image: [b, n2, h, w], extra ground truth relighted image for
      supervision.
# envmap: [b, 3, h_e, w_e]. target lighting environment map
# Output: training loss

# Step-1: geometry token extraction from input images
x_inp = concat([x_inp, x_inp.ray_plucker], dim=1) # [b, n, h, w, 9]
x_inp = conv1(x_inp, out=d, kernel=8, stride=8) # patchfy: [b, n, h/8, w/8, d]
x_inp = x_inp.reshape(b, -1, d) # [b, n_inp_tokens, d]
x_inp_geo = transformer1(LN(x_inp))

# step-2: tokenize envmap
e_darker = log(envmap) / max(log(envmap))
e_brighter = HLG(envmap) # hybrid log-gamma transfer function
x_light = concat([e_darker, e_brighter, envmap.ray_d], dim=-1) # [b, h_e, w_e, 9]
x_light = conv2(x_light, out=d, kernel=8, stride=8)
x_light = x_light.reshape(b, -1, d) # [b, n_light_token, d]
x_light = linear(GeLU(x_light), out=d) # [b, n_light_token, d]

# step-3: add noise to target_relit_image
t = randint(0, 1000, (x_inp.shape[0], )) # [b,]
alpha_cumprod = ddpm_scheduler(t)
noise = randn_like(target_relit_image)
x_t_relight = target_relit_image * sqrt(alpha_cumprod) + noise * sqrt(1 -
      alpha_cumprod)
t_token = TimeStepEmbedder(t) # [b, 1, d]

# step-4: tokenize noisy relit images
# concate with plucker ray of denosing views to [b, n', h, w, 9]
x_t_relight = concate([x_t_relight, target_relit_image.ray_plucker])
x_t_relight = conv3(x_t_relight, out=d, kernel=16, stride=16)
x_t_relight = x_t_relight.reshape(b, -1, d) # [b, n_relight_token, d]

# step-5: feed every tokens to the denosing transformer
# everything as tokens
x_all = concat([x_inp_geo, x_light, x_t_relight, t_token], dim=1)
# [b, n_inp_tokens + n_light_tokens + n_relight_tokens + 1, d]
x_all = transformer2(LN(x_all))
x_inp_radiance, _ = x_all.split(x_inp_geo.shape[1], dim=1) # [b, n_inp_token, d]

# step-6: decode pixel-algined 3D Gaussian parameters
# geometry parameters
x_geo = x_inp_geo.reshape(b, n, h//8, w//8, d)
x_geo = deconv(LN(x_geo), out=9, kernel=8, stride=8) # unpatchify to pixel-aligned GS
      output: [b, n, h, w, 9]
x_geo = x_geo.reshape(b, -1, 9) # all geometry params [b, n * h * w, 9]
# apperance_parameters, spherical-harmonics up to order of 4
x_inp_radiance = x_inp_radiance.reshape(b, n, h//8, w//8, d)
sh_weight = deconv(LN(x_inp_radiance), out=75, kernel=8, stride=8) # 75-dim sh

# GS parameterization
distance, scaling, rotation, opacity = x_geo.split([1, 3, 4, 1], dim=-1)
w = sigmoid(distance)
xyz = x_inp_ray_o + x_inp_ray_d * (near * (1 - w) + far * w)
scaling = min(exp(scaling - 2.3), 0.3)
rotation = rotation / rotation.norm(dim=-1, keepdim=True)
opacity = sigmoid(opacity - 2.0)

# step-7: compute training loss
3dgs = (xyz, rgb, scaling, sh_weight, rotation, opacity)

pred_x0, pred_extra_view = Render(3dgs, [target_relit_image.camera, extra_train_image
      .camera])

l2_loss = L2([pred_x0, pred_extra_view], [target_relit_image, extra_train_image])
lpips_loss = LPIPS([pred_x0, pred_extra_view], [target_relit_image, extra_train_image
      ])
loss = l2_loss + 0.5 * lpips_loss
```

A.2 Model details

Tokenizing HDR environment maps. To make it easier for networks to ingest HDR environment maps $E \in \mathcal{R}^{H_e \times W_e \times 3}$, we convert each E into two feature maps through two different tone-mappers: one E_1 emphasizing dark regions and one E_2 for bright regions.

$$E_1 = \frac{\log_{10}(E)}{\max(\log_{10}(E))}, \quad E_2 = \mathrm{HLG}(E), \tag{9}$$

where $\mathrm{HLG}(\cdot)$ represents the hybrid log-gamma transfer function. We then concatenate E_1, E_2 with the ray direction D, creating a 9-channel feature for each environment map pixel. Then we patchify it and apply a two layer MLP with to turn it into light tokens, $\{\boldsymbol{T}_{ij}^{\text{light}}\}_{j=1,2,\ldots,H_e W_e/p_e^2}$.

A.3 Image and Lighting preprocessing

To address scale ambiguity in relighting, we normalize both the rendered images and the environment map lighting in the dataset. For a rectangular target environment map, we compute its total energy, weighted by the sine of each pixel's elevation angle. We then normalize the environment map to ensure the weighted total energy matches a predefined constant. The same scaling factor is applied to the HDR rendered images. The detailed process is outlined in pseudo code 2.

Algorithm 2 Normalize environment map and rendered images .

```
# normalize the rendered images and environment maps
# Input list:
# x: [n, h, w, 3], n is number of views rendered for this scene under this lighting.
    h is image widht and w is image height.
# envmap: [h_e, w_e, 3]. environment map used to render this scene.
# constant_energy: pre-defined total energy. precomputed as dataset median number
# output list: x_normalized, envmap_normalized

# Step-1: compute weighted total energy of the environment map
H, W = envmap.shape[:2]
theta = linspace(0.5, H - 0.5, H) / H * np.pi
sin_theta = sin(theta)
envmap_weighted = envmap * sin_theta[:, None, None]
weighted_energy = sum(envmap_weighted)

# step-2: compute scaling factor
scale = constant_energy / weighted_energy

# step-3: normalize envmap
envmap = envmap * scale

# step-4: normalize and tonemap rendered images
x = x * scale # [n, h, w, 3]
x_flatten = x.reshape(-1, 3) # [n_total_pixel, 3]
x_min, x_max = percentile(x_flatten, [1, 99])
x = (x - x_min) / (x_max - x_min)
x = x.clip(0, 1)
# tonemapping
x = x ** (1.0 / 2.2)

return x, envmap
```

A.4 Training hyperparameters

We begin by training the model from scratch with four input views, four denoising views, and two additional supervision views under target lighting, at a resolution of 256×256. The model is trained for 80K iterations with a batch size of 512, using the AdamW optimizer with a peak learning rate of $4e-4$ and a weight decay of 0.05. The β_1, β_2 are set to 0.9 and 0.95 respectively. We use 2000 iterations of warmup and start to introduce perceptual loss after 5000 iterations for training stability. We then finetune the model at a resolution of 512×512 with six input views, six denoising views, and two supervision views, increasing the number of input tokens to 31K. This finetuning runs for 20K iterations with a batch size of 128, using the AdamW optimizer with a reduced peak learning rate of $4e-5$ and 1000 warmup steps. Throughout training, we apply gradient clipping at 1.0 and skip steps where the gradient norm exceeds 20.0.